3D Ultrasound Volume Stitching Using Phase Symmetry and Harris Corner Detection for Orthopaedic Applications

Rupin Dalvi[a1] Ilker Hacihaliloglu[a], Rafeef Abugharbieh[a]

[a] Biomdedical Signal and Image Computing Laboratory, Department of Electrical and Computer Engineering, University Of British Columbia (UBC)

ABSTRACT

Stitching of volumes obtained from three dimensional (3D) ultrasound (US) scanners improves visualization of anatomy in many clinical applications. Fast but accurate volume registration remains the key challenge in this area.We propose a volume stitching method based on efficient registration of 3D US volumes obtained from a tracked US probe. Since the volumes, after adjusting for probe motion, are coarsely registered, we obtain salient correspondence points in the central slices of these volumes. This is done by first removing artifacts in the US slices using intensity invariant local phase image processing and then applying the Harris Corner detection algorithm. Fast sub-volume registration on a small neighborhood around the points then gives fast, accurate 3D registration parameters. The method has been tested on 3D US scans of phantom and real human radius and pelvis bones and a phantom human fetus. The method has also been compared to volumetric registration, as well as feature based registration using 3D-SIFT. Quantitative results show average post-registration error of 0.33mm which is comparable to volumetric registration accuracy (0.31mm) and much better than 3D-SIFT based registration which failed to register the volumes. The proposed method was also much faster than volumetric registration (~4.5 seconds versus 83 seconds).

Keywords: 3D image registration, ultrasound volume stitching, computer assisted surgery, orthopaedics

1. INTRODUCTION

Ultrasound (US) is one of the safest and cheapest imaging modalities available today and is becoming increasingly popular as a valuable non-ionizing and portable real time alternative to intra-operative fluoroscopy in computer-assisted orthopaedic surgery (CAOS) applications. Nevertheless, extraction of relevant anatomical information from US images continues to be very challenging as such data typically contains significant speckle and other artifacts that complicate image interpretation and automatic processing. Furthermore, the very limited field of view (FOV) of acquired images makes the interpretation of the anatomical structures being imaged very difficult. Ultrasound volume stitching techniques aim to address this by combining the information of several US images taken from different directions. Three dimensional (3D) US volume stitching has been the subject of some recent research work. Meyer [1] used mutual information to provide affine and elastic registrations of 3D US volumes. Krücker [2] modified [1] using a sub-volume approach for faster registration. Pratikakis et al. [3] combined the minimization scheme of an automatic 3D non-rigid registration method with a multi-scale framework to register 3D US volumes. Poon et al. [4] attempted volume stitching of 3D US volumes obtained from a tracked probe. The obtained volumes were compounded using the tracking parameters and the residual errors were corrected using two different block-based registration methods. Wachinger et al. [5] proposed simultaneous global alignment of multiple ultrasound volumes based on a maximum likelihood framework. Ni et al. [6] proposed feature based alignment by registration of features obtained from the 3D US volumes using the 3D scale invariant feature transform (SIFT). Registration of multiple freehand 3D US volumes (obtained from freehand sweeps) was attempted by Gee et al. [7]. Instead of registering the entire volume, they registered the volumes only at the dividing plane in order to improve registration speed. In a more unusual application of 3D US volume registration Pennec et al. [8] aligned 3-D US brain volumes using a radial basis parameterization.

All these previous works involve some form of elastic warping of the volumes to align them. Hence, many of them are time intensive and also are prone to registration errors, since a volume may be warped in more than one way to closely fit another. However, most of them deal with applications where deformable registration is necessary. In orthopaedic

---

[1] Email: rupind@ece.ubc.ca . URL: http://bisicl.ece.ubc.ca/. Tel: + 1 604 822-8851. Fax: +1 604 822-5949

applications, such as CAOS or joint tracking, the tissue being registered is usually bone, which removes, or at least alleviates, some of the need for deformable registration. However, the presence of reverberations, shadows, speckles etc. in ultrasound data presents a challenge, even in rigid registration frameworks and often leads to poor performance when using intensity-based metrics such as sum of squared differences, normalized cross-correlation and mutual information. Furthermore, since the intensity of the same structure may differ from one ultrasound scan to another depending on the probe orientation, the intensity based registration algorithms are largely affected by inter-scan intensity variations.

Traditionally, feature based registration has been discounted for US registration, due to the difficulty in locating salient feature point correspondences between volumes. However, Hacihaliloglu et al. [9] showed that Log-Gabor filters can be used in a multi resolution scheme to significantly improve the signal to noise ratio in US images of bone tissue localization purposes. Moreover, recently, the SIFT algorithm by Lowe [10], has been successfully used by Chen et al. [11] for rapid feature based preregistration of multi-modal images. Ni et al. [6] have used 3D SIFT features to successfully register 3D US volumes for stitching purposes. Though their algorithm takes about a minute to register the volumes, they prove that feature based registration is a valid option for 3D US alignment.

In this paper, we use probe tracking, Log-Gabor filters, Harris corner detection and sub-volume registration to obtain fast and accurate rigid registration which we use for stitching ultrasound volumes of bone tissue. The tracked probe enables initial coarse registration between the two volumes and hence the central slices of the volumes contain similar structures. These central slices are then filtered using Log-Gabor filters to extract intensity invariant local phase features. Subsequently, Harris corner features are identified in each slice and matched to corresponding points in the other slice, and the best matching point pair is selected. Finally, sub-volumes around these two points are registered on a volumetric basis using mutual information as a metric and gradient descent as an optimizer. The resulting registration parameters are then used to determine the registration parameters for the entire volume.

We validate our proposed method on volumes obtained by scanning phantom and in vivo human radii, phantom pelvis bones and an artificial human fetus.

2. METHOD

The first step in our algorithm is to use the parameters obtained from the probe tracking for generating an initial coarse volume registration. Once this is done, the central slices will contain many corresponding features. Before identifying these features, we process the data to reduce noise effects and to boost the bone signal-to-noise-ratio in these central slices.

In a recent work, Hacihaliloglu et al. [10] proposed the use of Log-Gabor filters for extracting ridge-like features similar to those that occur at soft tissue/bone interfaces. The purpose of ridge detection was to capture the major axis of symmetry. In order to extract symmetric features that are intensity invariant, Hacihaliloglu et al. used local phase image information by defining a measure of phase symmetry (PS) to enhance the bone tissue interface.

Symmetric features can be decomposed into a set of even Fourier components centered on the point of symmetry. The phase and amplitude of a 1D signal $I(x)$ can be obtained by convolving the signal with a pair of band-pass quadrature filters (an odd filter and an even filter). At a point of symmetry on the scale of the spatial extent of the filters, the response of the even filter will dominate the response of the odd filter. In 1D, the odd filter can be obtained by taking the Hilbert transform of the even filter. Using two filters in quadrature enables the amplitude and phase of the signal to be calculated for a particular scale and frequency at a given spatial location. A good choice for the quadrature filters is the Log-Gabor filter [13] which can be constructed with arbitrary bandwidth. Analysis of the symmetric points of the signal can thus be done by constructing a filter bank using a set of these quadrature filters created from rescalings of the Log-Gabor filter. Each scaling is designed to pick out particular frequencies of the signal being analyzed. The 1D Log-Gabor filter can be extended to 2D by masking the Log-Gabor function with an angular Gaussian tuned to ϕ_0. which corresponds to the orientation of the filter. The 2D Log-Gabor filter is then defined as:

$$G(\omega,\phi) = \exp[-(\frac{(\log(\omega/\omega_0))^2}{2(\log(\kappa/\omega_0))^2} + \frac{(\phi-\phi_0)^2}{2\sigma_\phi^2}]$$

(1)

The scaling of the radial Log Gabor function is achieved by using different wavelengths that are based on multiples of a minimum wavelength, λ_{min}, which is a user-defined parameter. The relationship between the filter scale m, and the filter

center frequency ω_0 is set as $\omega_0 = 1/\lambda_{min} \times (\delta)^{m-1}$ where δ is a scaling factor defined for computing the center frequencies of successive filters. $\sigma_\phi = \Delta\phi/s$ defines the angular bandwidth $\Delta\Omega = 2\ \sigma_\phi\ (2\log2)^{-05}$ where $\Delta\phi$ is the angular separation between neighbouring orientations and is defined as $\Delta\phi = 180°/N_r$, and N_r denotes the total number of orientations used. The parameter s is the standard deviation of the Gaussian spreading function in the angular direction that describes the filter's angular selectivity. To obtain higher orientation selectivity, the angular function must become narrower. Steering of the filter is achieved by changing its angle (ϕ_0). The reader is referred to [10] for more details about the filter parameters and how they are set during the construction of a Log-Gabor filter bank.

Local phase symmetry extraction from a 2D US image, $I(x,y)$, can thus be obtained by convolving $I(x,y)$ with the 2D Log Gabor filters. Let $\hat{H}(u,v)$ be the Fourier transform of $I(x,y)$, we can think of the responses of each quadrature pair of filters as forming a response vector $[e_{rm}(x,y),o_{rm}(x,y)]=[real(\mathbf{F^{-1}}(\hat{H}(u,v)\ G(\omega,\phi_r))),\ imag\ (\mathbf{F^{-1}}(\hat{H}(u,v)\ G(\omega,\phi_r)))]$. Here $\mathbf{F^{-1}}$ denotes the inverse Fourier transform operation.

The 2D phase symmetry measure is thus defined for different scales (m) and orientations (r) as:

$$PS(x,y) = \frac{\sum_r \sum_m \lfloor [|e_{rm}(x,y)| - |o_{rm}(x,y)|] - T_r \rfloor}{\sum_r \sum_m \sqrt{e_{rm}^2(x,y) + o_{rm}^2(x,y)} + \varepsilon} \qquad (2)$$

Here $\lfloor A \rfloor = \max(A,0)$, ε is a small number included to avoid division by zero, and T is a noise threshold calculated as a specified number (k) of standard deviations (σ) above the mean (μ) of the local energy distribution [10]. Fig. 1 shows example PS images obtained by processing B-mode US images obtained by scanning an *in-vivo* human distal radius. It can be clearly seen that the PS image accurately localizes the bone boundary.

(a) Central slice of Volume 1

(b) Central slice of Volume 2

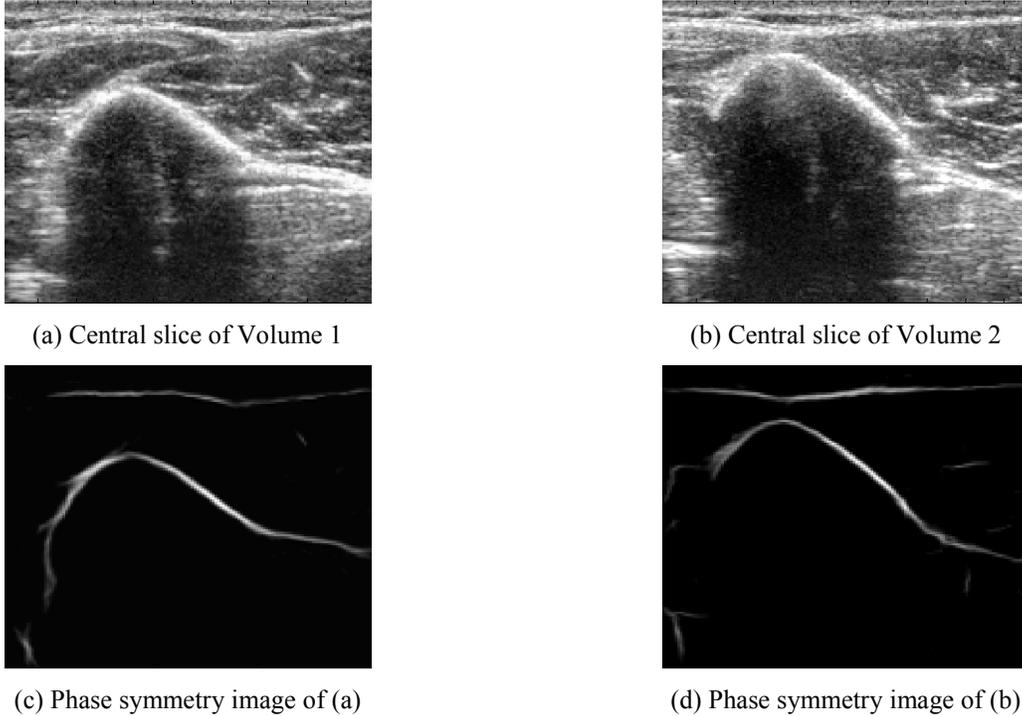(c) Phase symmetry image of (a)

(d) Phase symmetry image of (b)

Fig. 1: Central slices of the two volumes (in vivo distal radius) to be registered and their corresponding phase symmetry images

Once the US image is processed and the bone surface made prominent (Fig. 1), the Harris corner detection algorithm [13] is used to obtain features in both slices. Given a phase processed image I_p, we consider two image windows, one covering an area of size $a \times b$ and the other covering the same area shifted from the first by (x,y). The sum of squared differences (SSD) for these two windows is defined as:

$$SSD(x,y) = \sum_a \sum_b w(a,b)(I_p(a,b) - I_p(a+x,b+y))^2 \tag{3}$$

where $w(a,b)$ is a weighting factor.

$I_p(a+x,b+y)$ can be approximately written as:

$$I_p(a+x,b+y) \approx I_p(a,b) + I_{p_x}(a,b)x + I_{p_y}(a,b)y \tag{4}$$

where I_{px} and I_{py} are partial derivatives of I_p. Thus, the SSD is given as:

$$SSD(x,y) \approx (x \quad y)A\binom{x}{y} \tag{5}$$

where

$$A = \sum \sum w(a,b)\begin{bmatrix} I_{p_x}^2 & I_{p_x}I_{p_y} \\ I_{p_x}I_{p_y} & I_{p_y}^2 \end{bmatrix} \tag{6}$$

The eigenvalues of A (λ_1 and λ_2) are then used to determine corner points:

If $\lambda_1 \approx 0$ and $\lambda_2 \approx 0$, then pixel (x,y) has no features of interest.

If $\lambda_1 \approx 0$ and λ_2 has large positive value, then pixel (x,y) is on an edge.

If λ_1 and λ_2 have large positive values, then pixel (x,y) is a corner.

A RANSAC algorithm [14] is used to remove outliers and to find reliable correspondences between the feature points obtained in the two slices. For each matching point pair $p = (m,n)$, windows of size r (in our case 29×29) around each point are determined and the correlation C_p between them is calculated. The point pair with maximally correlating neighbourhoods is selected as a salient point pair (Fig. 2)
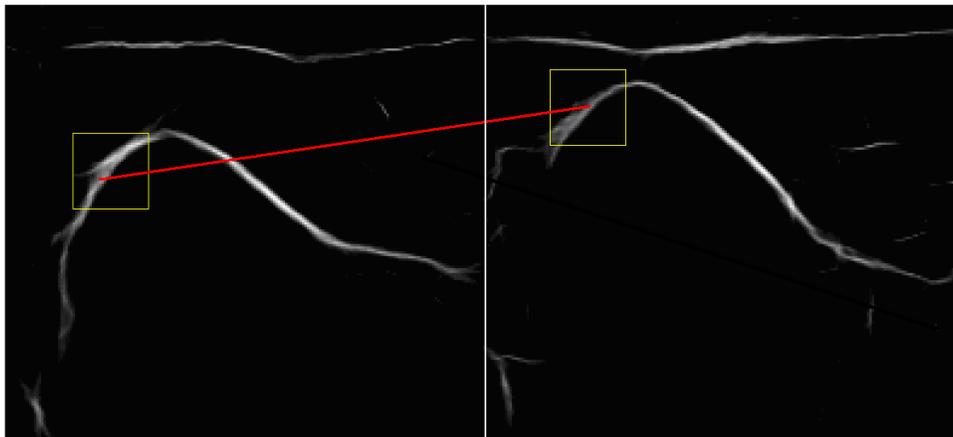

Fig. 2: Salient Point Selection. The corresponding points shown in the two sub-windows are the points around which the sub-volumes to be registered are formed.

Once the salient point pair is identified, sub-volumes around the points are generated in both volumes and rigidly registered using rigid volumetric registration, with normalized cross correlation being used as a metric and gradient descent as an optimizer. Once the parameters for the registration of the two sub-volumes are obtained, they are used to obtain the transformation parameters that are to be used on the whole image volumes.

Implementation Details

During the construction of Log-Gabor filter we used two scales (m=2) with a large wavelength (λ_{min}= 25) and a scaling factor of δ=3. A value of κ/ω_0 =0.25 provided good surface localization in the presence of speckle. For the angular component, we found empirically after some experimentation with models of the human distal radius and pelvis that it was possible to get good orientation resolution while containing an adequate range of frequencies by selecting an angular bandwidth value σ_α=25°. The filter bank used in this work used 6 different filter orientations. The noise threshold parameter k was set to 5. In all the quantitative validation experiments these selected filter parameters were not changed. The sub volume size during the calculation of the registration was 39.3 mm^3 (17×17×17 pixels) which was empirically set to balance registration time and accuracy.

3. EXPERIMENTS AND RESULTS

The method was tested on two real (in vivo) human radius bones, two artificial human distal radius bones (Sawbone Model #1018-3, Sawbones Inc., Vashon, WA, USA), a real in-vitro bovine femur, an artificial fetus (CIRS, Inc., Norfolk, VA, USA), and an artificial human pelvis (Sawbone Model #1301-96, Sawbones Inc., Vashon, WA, USA). In the case of the artificial bones (radius and pelvis), four fiducials were attached to the bones at regular intervals for quantitative assessment. The distance between the fiducials in the stitched volumes was compared to the actual distance on the physical bones and the accuracy of the stitching was subsequently computed.

$$Error = \left| Dist_{True} - Dist_{Stitched} \right| \qquad (7)$$

$Dist_{True}$ = Mean actual distance between fiducials on the physical objects

$Dist_{Stitched}$ = Mean distance between fiducials in the stitched volumes

Table 1: Mean error measurements (based on 4 fiducials) for stitching bones. The distance between the fiducials in the stitched volumes was compared to the actual distance on the physical bones and the accuracy of the stitching was subsequently computed. Any error greater than 5mm has been thresholded at 5mm.

	Fiducial Error (mm)				
Bone	Error before registration (tracking only)	Error after tracking and proposed registration with Harris	Error after Volumetric Registration	Error after tracking and proposed registration with SIFT	Error after tracking and 3D-SIFT based registration
Phantom distal radius 1	3.15	0.59	0.55	5	5
Phantom distal radius 2	1.47	0.37	0.33	5	5
Ex vivo bovine femur	0.84	0.28	0.33	5	5
Phantom pelvis	0.25	0.05	0.04	5	5

The results of the algorithm on the in vivo, real radius scans were only assessed qualitatively by visual inspection since there was no ground truth data. Our images were scanned using a GE Voluson 760 US scanner. The algorithm was implemented in MATLAB (The MathWorks, Inc., MA, UNITED STATES) except for the sub volume registration step,

for which ITK (Kitware, Inc., NY 12065 USA) was used. The algorithm was run on a P4 system with 2GB of RAM with our registration requiring, on average, 4.5 seconds (for 2 volumes).

In lieu of a tracking system, the volumes were obtained by moving the probe along a straight line for known distances (0.5 cm) between scans and then these distances were used as tracking parameters. The quantitative results are shown in Table 1 and the qualitative results for the artificial radius and fetus scans are shown in Figure 3.

We compared our method against volumetric registration to test for accuracy and speed differences. The volumetric registration used Mutual Information as a registration metric and a Gradient Descent optimiser. We also compared the method to feature based registration using 3D-SIFT. The 3D-SIFT feature based registration method obtained features in both volumes and used them to register the volumes to each other. Finally, we compared the performance of the Log-Gabor+Harris corner detector to the SIFT feature detector when used in the proposed method's framework.

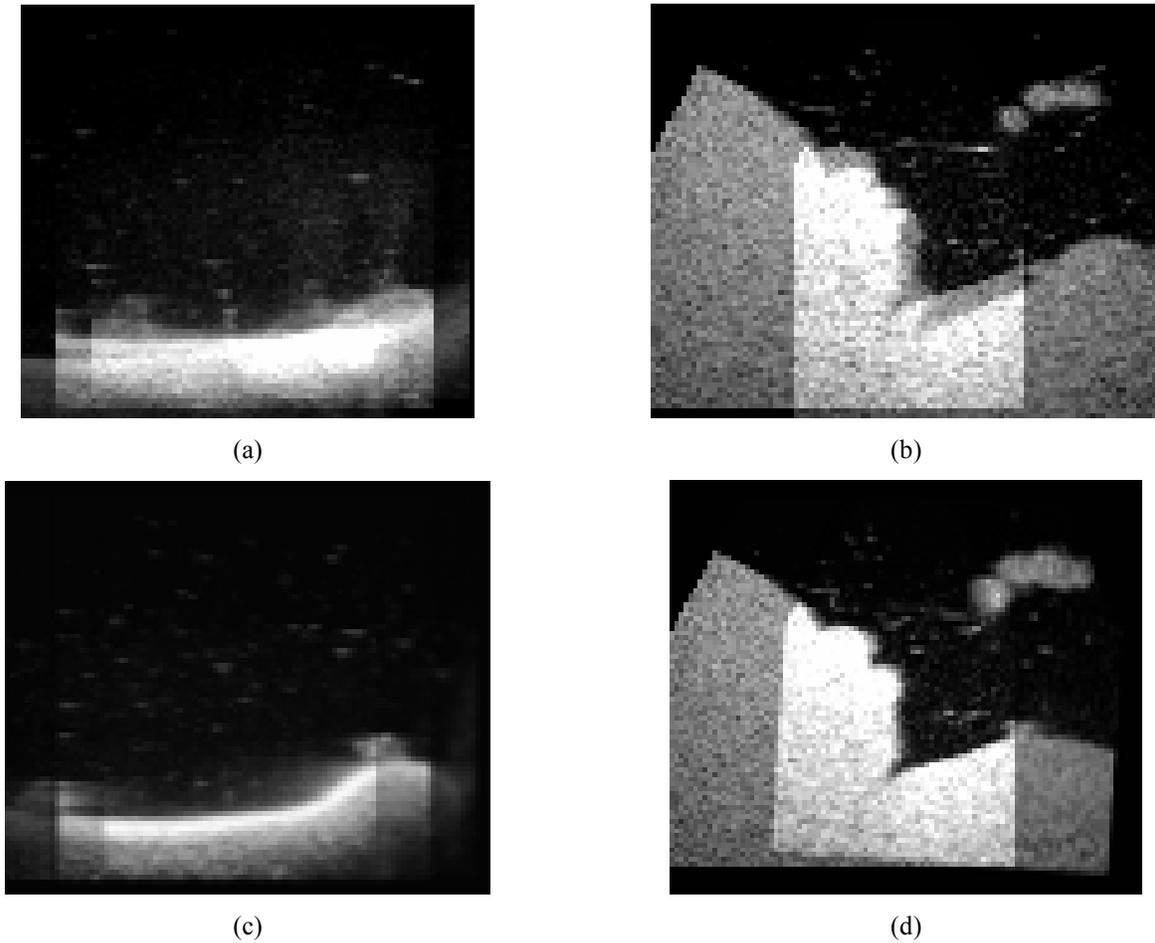(a)　　　　　　　　　　　　　　　　　　(b)

(c)　　　　　　　　　　　　　　　　　　(d)

Figure 3: Qualitative assessment of the registration of the distal radius phantom(left) and the fetus phantom (right) for volume stitching. (a) and (b) shows stitching before registration, i.e. using only the probe tracking. (c) and (d) show the results of stitching after tracking and proposed registration. It can be clearly seen that the registered stitched volumes have no discontinuities which can be seen in the unregistered ones. Note that the stitching was achieved by merely adding the registered volumes together, hence the region of overlap is seen to be much brighter than the surroundings.

The results for all the methods on the fiducial embedded bones are compared in Table 1. As can be seen, the proposed method's performance is comparable to the volumetric registration method in terms of accuracy. However, it takes only

4.5 seconds on average to register the two volumes as opposed to the volumetric method, which takes about 83 seconds to perform the registration.

The proposed method significantly outperforms both SIFT-based methods. The 2D-SIFT feature detector, when used instead of the Log-Gabor+Harris detector, performs very poorly on bone US data, returning mostly incorrect matches. The 3D-SIFT also finds very few matches across both volumes, and they are also often incorrect. As can be seen from Table 1, both methods failed to register the images/volumes in all cases (the 5mm error shown in the table indicates complete failure to register; any error more than 5mm is depicted as 5mm). This may be due to the fact that the SIFT detector is not tuned for detecting features along edges/ridges, which are precisely the anatomical structures that are being imaged here.

(a)   (b)
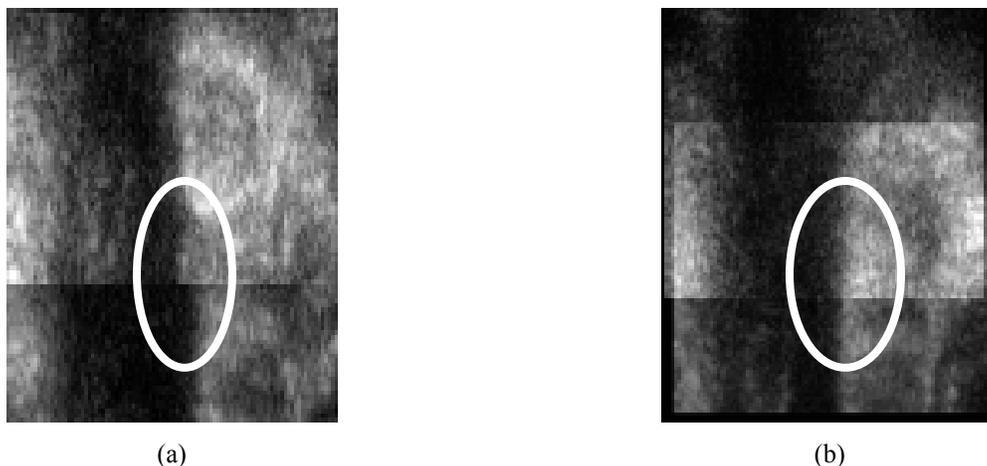
Figure 4: Qualitative assessment of the registration for the in vivo radial scans for volume stitching. Here, (a) indicates stitching before registration, using only the tracking and (b) shows the results of stitching after tracking and registration. The dark region is actually the shadow region below the bone – it was shown rather than the bone itself since the discontinuity at the overlap in (a) (circled) is more clearly highlighted in this region. Note the smooth transition in (b). The stitching was achieved by merely adding the registered volumes together; hence the region of overlap is seen to be much brighter than the surroundings.

4.   CONCLUSIONS AND DISCUSSION

The ability to perform intra-operative registration accurately, automatically, and rapidly is of critical importance for enabling more effective image guidance. In this paper we proposed a novel registration scheme for fast and accurate registration enabling 3D US volume stitching. The method registers US volumes with high accuracy (average registration error of 0.33mm), which is comparable to that of volumetric registration (error of 0.31mm), while providing a significant advantage in speed (4.5 seconds versus 83 seconds). Extracting features from intensity invariant local phase images makes the method more robust to typical US artifacts where popular methods such as SIFT seem to have difficulties. One of the possible future applications of the proposed scheme could be registering pre-operative CT data to intra-operative US which is one of the main topics of research in CAOS systems. Future work will focus on testing of the algorithm on various orthopaedic data as well as on optimizing the code to achieve real time operation.

REFERENCES

[1] Meyer, C., Boes, J., Kim, B., Bland, P., LeCarpentier, G., Fowlkes, J., Roubidoux, M., Carson, P., "Semiautomatic registration of volumetric ultrasound scans." *Ultrasound Med. Biol.*, 25, 339–347, (1999).
[2] Krücker, J., LeCarpentier, G., Fowlkes, J., Carson, P., "Rapid elastic image registration for 3-D ultrasound." *IEEE Trans. Med. Imag.*, 21, 1384–1394, (2002).

[3] Pratikakis, I., Barillot, C., Hellier, P., Mémin, E., "Robust multiscale deformable registration of 3-D ultrasound images." Int. J. Image Graphics, 3(4), 547-566 (2003)

[4] Poon, T., Rohling, R., "Three-dimensional extended field-of-view ultrasound." Ultrasound in Medicine and Biology 32(3), 357–369, (2003).

[5] Wachinger, C., Wein, W., Navab, N., "Three-dimensional ultrasound mosaicing." MICCAI, 4792, 327–335, (2007).

[6] Dong Ni, Yingge Qu, Xuan Yang, Yim-Pan Chui, Tien-Tsin Wong, Simon S. M. Ho, Pheng-Ann Heng, "Volumetric Ultrasound Panorama Based on 3D SIFT." MICCAI 2008, 52-60, (2008).

[7] Gee, A., Treece, G., Prager, R., Cash, C., Berman, L., "Rapid registration for wide field of view freehand three-dimensional ultrasound." IEEE Trans. Med. Imaging 22(11), 1344–1357, (2003).

[8] Pennec, X., Cachier, P., Ayache, N., "Tracking brain deformations in time-sequences of 3-D US images." *Pattern Recogn. Lett.*, 24, 801–813, (2003).

[9] Hacihaliloglu, I., Abugharbieh, R., Hodgson, A.J., Rohling, R.N., "Bone surface localization in ultrasound using image phase based features." *Ultrasound Med. Biol.*, 35, 1475-1487, (2009).

[10] Lowe, D., "Distinctive image features from scale-invariant keypoints." International Journal of Computer Vision 60(2), 91-110, (2004).

[11] Chen, J., & Tian, J., "Rapid Multi-modality preRegistration based on SIFT descriptor." Engineering in Medicine and Biology Society, (2006).

[12] Kovesi, P., "Symmetry and Asymmetry from Local Phase." Tenth Australian Joint Conference on Artificial Intellegence, 185–190, (1997)

[13] Harris, C., Stephens, M., "A combined corner and edge detector." *Proceedings of the 4th Alvey Vision Conference,* 147—151, (1988).

[14] Fischler, M., Bolles, R.: Random Sample Consensus, "A Paradigm for Model Fitting with Applications to Image Analysis and Automated Cartography." Comm. of the ACM, 24, 381-395, (1981).